Supplementary Information for

Excitation and Emission Distinguished Photoluminescence Enhancement in a Plasmon-Exciton Intermediate Coupling System

Wenjun Zhang,[a,b] Long Gao,[b,c] Xiaohong Yan,[b,d] Hongxing Xu*[a,e] and Hong Wei*[b,f]

[a]*School of Physics and Technology, Center for Nanoscience and Nanotechnology, and Key Laboratory of Artificial Micro- and Nano-structures of Ministry of Education, Wuhan University, Wuhan 430072, China*

[b]*Beijing National Laboratory for Condensed Matter Physics, Institute of Physics, Chinese Academy of Sciences, Beijing 100190, China*

[c]*Institute of Microscale Optoelectronics, Shenzhen University, Shenzhen 518060, China*

[d]*School of Physical Sciences, University of Chinese Academy of Sciences, Beijing 100049, China*

[e]*School of Microelectronics, Wuhan University, Wuhan 430072, China*

[f]*Songshan Lake Materials Laboratory, Dongguan 523808, China*

*E-mail: hxxu@whu.edu.cn; weihong@iphy.ac.cn

1. Experimental methods

Gold film of 200 nm thickness was deposited on a silicon substrate by electron beam evaporation. Then Al_2O_3 of 6 nm thickness was deposited on the gold using atomic layer deposition. After that, monolayer MoS_2 grown by chemical vapor deposition (6 Carbon Technology, Shenzhen) was transferred by polymethyl methacrylate (PMMA) onto the Al_2O_3 layer, followed by drop-casting chemically synthesized silver NWs with an accompanied thin coating layer of polyvinylpyrrolidone (PVP). The sample was rinsed with deionized water and then dried with nitrogen gas. Finally, another Al_2O_3 layer of 6 nm thickness was deposited onto the sample immediately to prevent the silver NWs from degradation.

All of the optical measurements were performed via an upright microscope (BX51, Olympus) equipped with a spectrometer (Acton SP2500i, Princeton Instruments). White light from a

halogen lamp passed through a dark-field module and was focused onto the sample by a dark-field objective (100×, NA 0.90). The scattering light from the sample was collected by the same objective and directed to a charge-coupled device camera or the spectrometer. The spectrometer was set to collect the light from an area of ~1.6 μm^2 on the sample. The polarization-resolved dark-field scattering spectra were measured by using a rotatable polarizer (U-AN360P, Olympus). The reflection spectra from the sample areas with or without MoS_2 were measured by replacing the dark-field module with a bright-field module. The differential reflection ($\Delta R / R$) spectrum is defined as the difference of the reflection spectra from the gold film and from the MoS_2 on gold film over the reflection spectrum from the gold film.

The PL was excited by CW laser light of 633 nm or 532 nm wavelength and detected by the spectrometer after passing through a long pass filter to block the laser light. There may exist intrinsic blinking PL in the NPOM structures.[1] In order to remove the influence of the PL blinking, we repeatedly measured multiple PL spectra and cautiously chose the steady PL spectra with a low pump power of 19.2 μW. To study the polarization of PL emission, a half wave plate and a polarizer were placed after the long pass filter. 0° and 90° are defined as the directions corresponding to the polarization parallel and perpendicular to the NW, respectively. The PL spectra of the MoS_2 on gold film close to the NWOMs were measured under the same conditions.

2. The distribution of in-plane electric field component of the plasmon mode

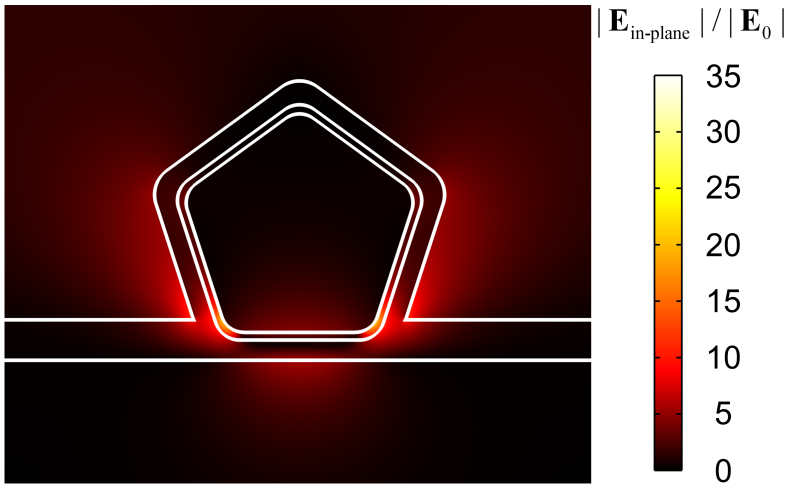

Fig. S1 The distribution of the in-plane electric field component of the plasmon mode for the NWOM with a NW diameter of 70 nm. The distribution of the total electric field is shown in the inset of Fig. 1d. The simulation was performed by the finite element method (see section 9 in the Supplementary Information).

3. Polarization-resolved scattering spectra of NWOM

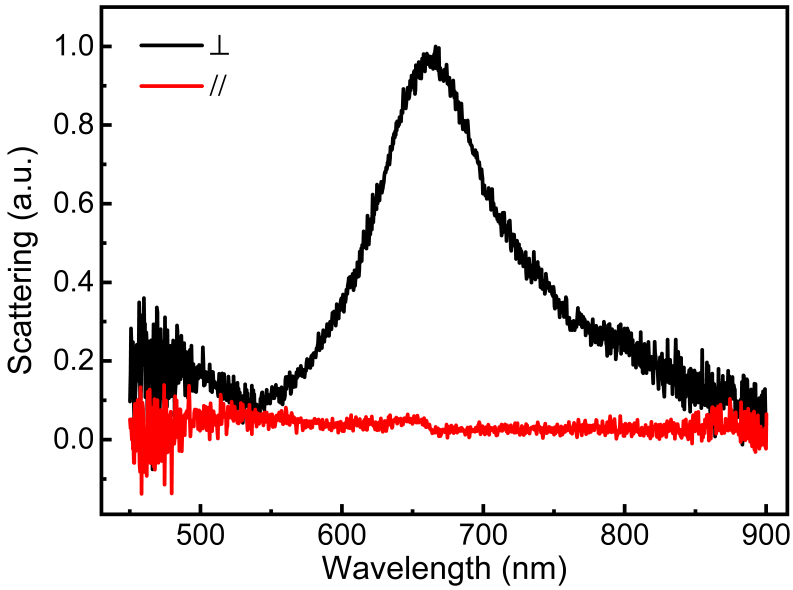

Fig. S2 Scattering spectra of a NWOM structure for scattering light polarized perpendicular (black) and parallel (red) to the NW.

4. Linewidth of the plasmon mode for NWOM as a function of plasmon energy

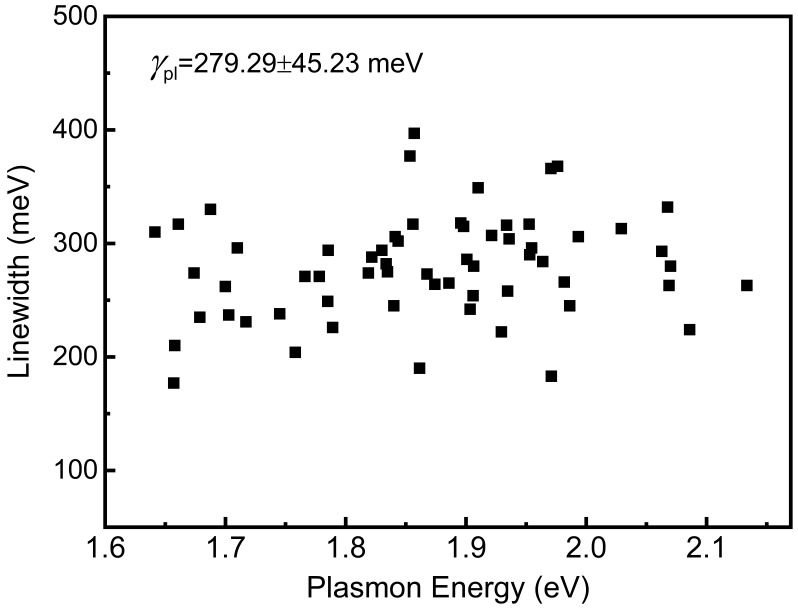

Fig. S3 Linewidth of the plasmon mode as a function of plasmon energy obtained by fitting the dark-field scattering spectra of NWOMs with one Lorentzian peak. The mean value and standard deviation of the linewidth is shown as inset.

5. Three-coupled-oscillators model

To fit the experimental energies of plexcitons, we utilized a three-coupled-oscillators model. The hybrid system of three coupled oscillators can be described by

$$\begin{pmatrix} E_{\mathrm{pl}} - i\frac{\gamma_{\mathrm{pl}}}{2} & g_{\mathrm{A}} & g_{\mathrm{B}} \\ g_{\mathrm{A}} & E_{\mathrm{A}} - i\frac{\gamma_{\mathrm{A}}}{2} & 0 \\ g_{\mathrm{B}} & 0 & E_{\mathrm{B}} - i\frac{\gamma_{\mathrm{B}}}{2} \end{pmatrix} \begin{pmatrix} \alpha \\ \beta \\ \varphi \end{pmatrix} = E \begin{pmatrix} \alpha \\ \beta \\ \varphi \end{pmatrix}, \tag{S1}$$

where E_{pl}, E_{A}, and E_{B} are the energies of the plasmon mode, A exciton, and B exciton, respectively; γ_{pl}, γ_{A}, and γ_{B} are the linewidths of the plasmon mode, A exciton, and B exciton, respectively; g_{A} and g_{B} are the coupling strengths of the plasmon mode with A exciton and B exciton, respectively; E is the eigenvalue of the energy for the plexcitons; α,

β, and φ are the Hopfield coefficients which satisfy $|\alpha|^2+|\beta|^2+|\varphi|^2=1$.

6. Determining plasmon energy of MoS_2-NWOM coupled system by NW diameter

The plasmon energies of the MoS_2-NWOM coupled systems obtained by the energy relationship of plasmon mode, excitons, and plexcitons (black squares in Fig. S4a) are similar to the plasmon energies of the NWOMs without MoS_2 obtained by the dark-field scattering spectra (red dots in Fig. S4a). Therefore, it is also reasonable to obtain the plasmon energies of the MoS_2-NWOM coupled systems by the linear relationship of plasmon resonance wavelength and NW diameter (Fig. 1f). In Fig. S4b, the energies of plexciton branches are replotted with the plasmon energies deduced from the NW diameter. From the fitting results in Fig. S4b, the coupling strengths of the plasmon mode with A exciton and B exciton are obtained as 63 meV and 58 meV, respectively. The minimal splitting between LPB and MPB and between MPB and UPB are about 118 meV and 106 meV, respectively. These values are very close to the values obtained from the fitting results in Fig. 2c.

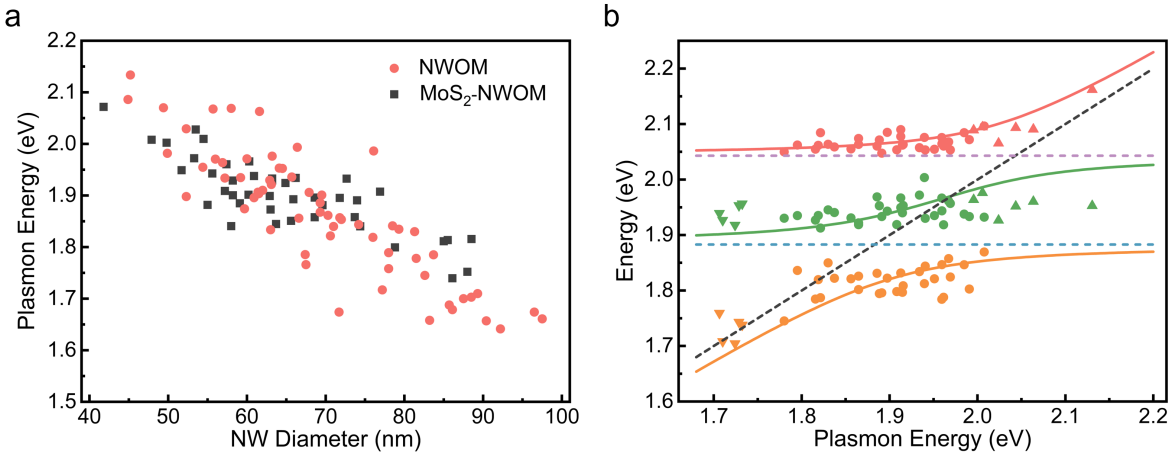

Fig. S4 (a) Plasmon energies of NWOMs obtained from the Lorentzian fitting of the scattering spectra (red dots) and of MoS_2-NWOMs obtained by the energy relationship of plasmon mode, excitons, and plexcitons (black squares) as a function of NW diameter. (b) Energies of plexciton branches as a function of plasmon energy obtained by the linear relationship of plasmon wavelength and NW diameter shown in Fig. 1f. The red, green, and orange circular dots represent experimental UPB, MPB, and LPB of A exciton-plasmon-B exciton coupling,

respectively. The red, green, and orange lines represent the fitting using the three-coupled-oscillators model. The green and orange inverted triangles represent experimental UPB and LPB of A exciton-plasmon coupling, respectively. The red and green upright triangles represent experimental UPB and LPB of B exciton-plasmon coupling, respectively. The blue, purple, and black dashed lines show the energies of A exciton, B exciton, and plasmon, respectively.

7. Linewidths of plexciton branches calculated from the three-coupled-oscillators model

The linewidth of each plexciton branch can be written as $\gamma_i = |\alpha_i|^2 \gamma_{\mathrm{pl}} + |\beta_i|^2 \gamma_{\mathrm{A}} + |\varphi_i|^2 \gamma_{\mathrm{B}}$, where the subscript *i* represents LPB, MPB, and UPB; $|\alpha_i|^2$, $|\beta_i|^2$, and $|\varphi_i|^2$ are the fractions of the plasmon mode, A exciton, and B exciton, respectively, for each plexciton branch, which are shown in Fig. 2d; γ_{pl}, γ_{A}, and γ_{B} are the linewidths of the plasmon mode, A exciton, and B exciton, respectively. Fig. S5 shows the linewidths of three plexciton branches. At the minimal splitting between LPB and MPB (E_{pl}=1.915 eV), γ_{LPB}=151 meV, γ_{MPB}= 165 meV. At the minimal splitting between MPB and UPB (E_{pl}=2.005 eV), γ_{MPB}=195 meV, γ_{UPB}=209 meV. By analogy with the strong coupling of two oscillators, the criterion for the strong coupling of multiple oscillators can be written as the minimal splitting between adjacent plexciton branches larger than their mean linewidth.[2] The minimal splitting between LPB and MPB (121 meV) and between MPB and UPB (105 meV) are both smaller than the mean linewidth of two corresponding plexciton states, indicating the system is in the intermediate coupling regime.

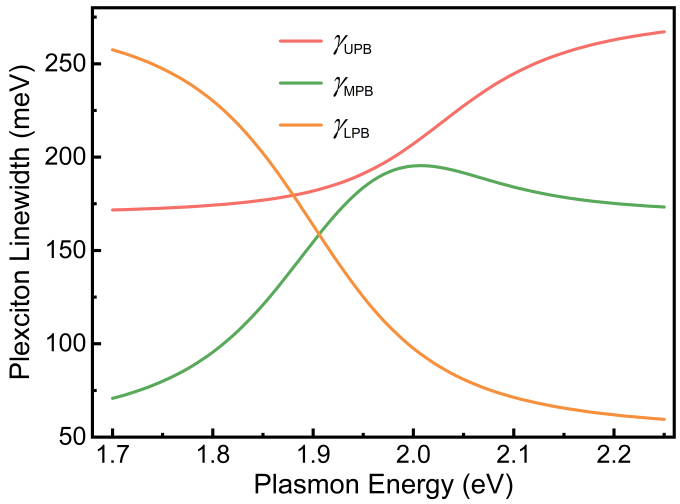

Fig. S5 Linewidths of three plexciton branches as a function of plasmon energy.

8. PL results of MoS_2-NWOM coupled systems

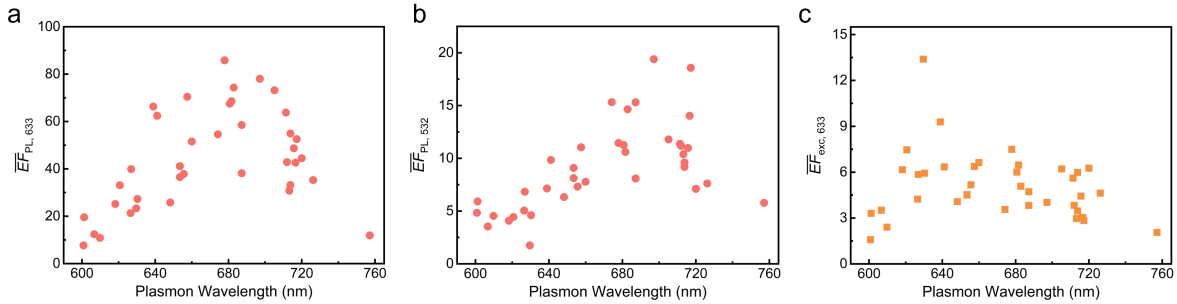

Fig. S6 (a and b) PL enhancement factor as a function of plasmon resonance wavelength for 633 nm excitation (a) and 532 nm excitation (b). (c) Derived excitation enhancement factor as a function of plasmon resonance wavelength for 633 nm excitation. The excitation light is polarized perpendicular to the NW.

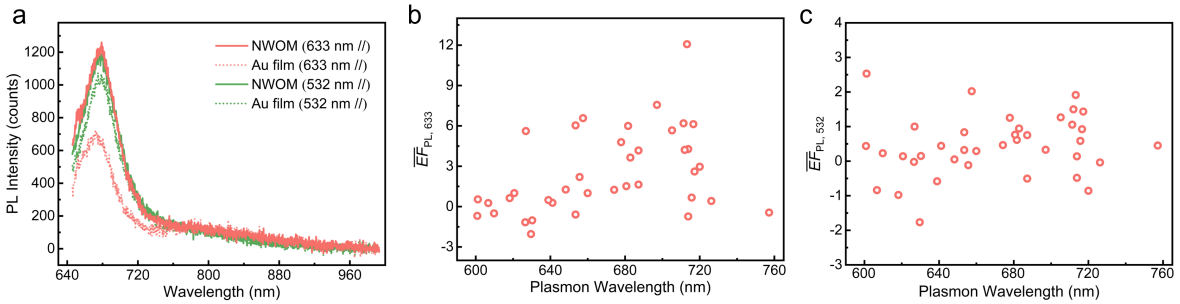

Fig. S7 (a) PL spectra of MoS_2 coupled with NWOM (solid lines) and on gold film (dot lines) for excitation light of 633 nm (red) and 532 nm (green) polarized parallel to the NW. (b and c) PL enhancement factor as a function of plasmon resonance wavelength for excitation light of

633 nm (b) and 532 nm (c) polarized parallel to the NW.

9. Simulations of scattering spectra, enhancement factors, and DOLP

Simulations were performed by the finite element method (COMSOL Multiphysics). The thicknesses of Al_2O_3, PVP, and MoS_2 layers are set to be 6 nm, 2.3 nm, and 0.7 nm, respectively. The structures are modeled with NWs of pentagonal cross-section, and the NW edges are filleted with a fillet radius of one tenth of NW diameter *D* to avoid local singularities and nonconverging electric field. The diameter *D* is varied from 45 nm to 95 nm. The refractive index of air is set to be 1 and the refractive indices of Al_2O_3 and PVP are based on the experimental results in literature.[3, 4] The refractive indices for gold and silver are based on the measurements of Johnson and Chrisity.[5] The out-of-plane permittivity of monolayer MoS_2 is 2.8,[6] and the in-plane component is obtained from fitting the experimental results in literature with the Lorentz oscillator model.[7]

To simulate the scattering spectra, the NWOM system with NW of infinite length is excited by a plane wave at normal incidence with polarization perpendicular to the NW. The power flow of the scattering field is integrated over the surface corresponding to the numerical aperture of the objective to obtain the scattering intensity of the system for each wavelength. Fig. S8 shows the simulated scattering spectra of NWOMs without MoS_2 and the corresponding plasmon resonance wavelengths for different NW diameters.

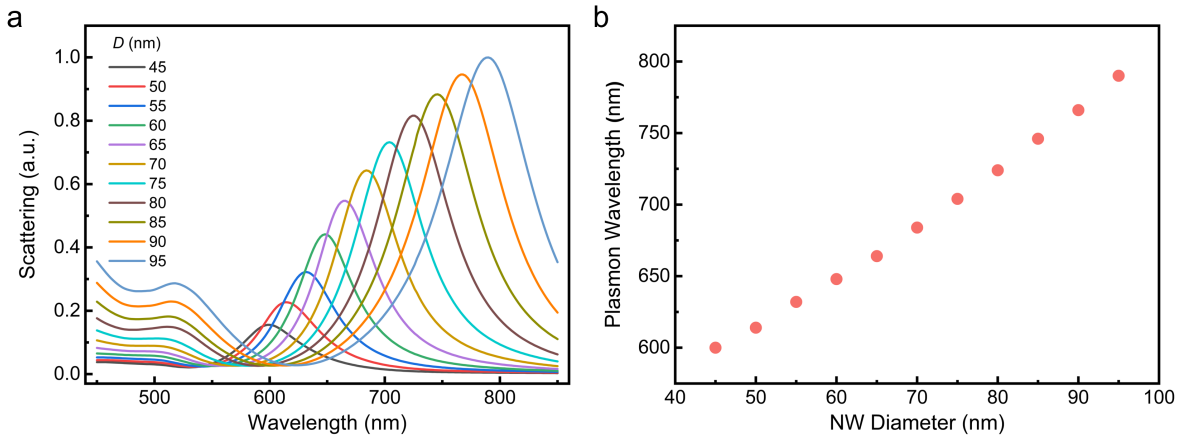

Fig. S8 (a) Simulated scattering spectra of NWOMs with different NW diameters *D*. (b) Plasmon resonance wavelength as a function of NW diameter.

In the simulation of the enhancement factor, the excitation and emission processes are modeled separately. In the excitation process, a Gaussian beam of 532 nm or 633 nm wavelength with beam radius of 350 nm is applied to excite the structure. For each point in the MoS_2 layer between the silver NW and gold film, the excitation enhancement factor can be expressed as $EF_{\text{exc}} = \dfrac{|\mathbf{E}_x + \mathbf{E}_y|^2}{|\mathbf{E}_{x,\text{film}} + \mathbf{E}_{y,\text{film}}|^2}$, where $\mathbf{E}_x$ and $\mathbf{E}_y$ are the components of the electric field in the central plane of MoS_2 layer in the nanogap perpendicular and parallel to the NW, respectively, and $\mathbf{E}_{x,\text{film}}$ and $\mathbf{E}_{y,\text{film}}$ are the corresponding components of the electric field in the central plane of MoS_2 layer on gold film without NW. The emission enhancement factor for each point can be expressed as $EF_{\text{emi}} = \dfrac{QY}{QY_{\text{film}}} \cdot \dfrac{\eta}{\eta_{\text{film}}}$, where QY and η are the quantum yield and collection efficiency of the PL for the exciton embedded in the NWOM structure, respectively, and QY_{film} and η_{film} are the corresponding quantities for the exciton on gold film without NW.

The intrinsic quantum yield of monolayer MoS_2 is expressed as $QY_0 = \dfrac{\gamma_{\text{rad},0}}{\gamma_{\text{rad},0} + \gamma_{\text{nrad},0}}$, where $\gamma_{\text{rad},0}$ and $\gamma_{\text{nrad},0}$ are the intrinsic radiative decay rate and nonradiative decay rate, respectively. The intrinsic nonradiative decay rate can then be written as $\gamma_{\text{nrad},0} = \dfrac{1-QY_0}{QY_0}\gamma_{\text{rad},0}$. It is assumed that the intrinsic nonradiative decay rate is not affected by the plasmonic nanostructure. When the exciton is in the plasmonic nanocavity, the quantum yield becomes $QY = \dfrac{\gamma_{\text{rad}}}{\gamma_{\text{rad}} + \gamma_{\text{nrad,m}} + \gamma_{\text{nrad},0}} = \dfrac{\gamma_{\text{rad}}}{\gamma_{\text{rad,X}} + \gamma_{\text{nrad},0}}$, where γ_{rad} and $\gamma_{\text{nrad,m}}$ are the radiative decay rate of the whole structure and the nonradiative decay rate caused by the silver NW and gold film, respectively; $\gamma_{\text{rad,X}}$ is the radiative decay rate of the exciton, and $\gamma_{\text{rad,X}} = \gamma_{\text{rad}} + \gamma_{\text{nrad,m}}$. Therefore, the enhancement of quantum yield can be expressed as

$$\frac{QY}{QY_{\text{film}}} = \frac{\gamma_{\text{rad}}}{\gamma_{\text{rad,film}}} \cdot \frac{\gamma_{\text{rad,X,film}} + \gamma_{\text{rad},0}(1-QY_0)/QY_0}{\gamma_{\text{rad,X}} + \gamma_{\text{rad},0}(1-QY_0)/QY_0}. \tag{S2}$$

The exciton is modeled as an oscillating current source with an emission wavelength of 680 nm, and the power radiated over an enclosed surface around the source in vacuum is defined as $P_{\mathrm{rad},0}$. For the exciton coupled with the NWOM, the power radiated over the enclosed surface Ω_{X} in Fig. S9 is defined as $P_{\mathrm{rad,X}}$. The collection efficiency can be expressed as $\eta = \frac{P_{\mathrm{rad,NA}}}{P_{\mathrm{rad}}}$, where P_{rad} is the radiated power of the whole system and $P_{\mathrm{rad,NA}}$ is the power radiated over the surface Ω_{NA} in the far-field domain which can be calculated from the near field using the Stratton–Chu formula. Because of $\frac{\gamma_{\mathrm{rad}}}{P_{\mathrm{rad}}} = \frac{\gamma_{\mathrm{rad,X}}}{P_{\mathrm{rad,X}}} = \frac{\gamma_{\mathrm{rad},0}}{P_{\mathrm{rad},0}}$,[8] the enhancement of quantum yield can be written as

$$\frac{QY}{QY_{\mathrm{film}}} = \frac{P_{\mathrm{rad}}}{P_{\mathrm{rad,film}}} \cdot \frac{P_{\mathrm{rad,X,film}} + P_{\mathrm{rad},0}(1-QY_0)/QY_0}{P_{\mathrm{rad,X}} + P_{\mathrm{rad},0}(1-QY_0)/QY_0}. \tag{S3}$$

Therefore, the emission enhancement factor can be written as

$$EF_{\mathrm{emi}} = \frac{P_{\mathrm{rad,NA}}}{P_{\mathrm{rad,NA,film}}} \cdot \frac{P_{\mathrm{rad,X,film}} + P_{\mathrm{rad},0}(1-QY_0)/QY_0}{P_{\mathrm{rad,X}} + P_{\mathrm{rad},0}(1-QY_0)/QY_0}. \tag{S4}$$

Considering the unpolarized emission from the monolayer MoS_2 on gold film, the emission enhancement can be simulated with two orientations (x and y) of the dipole moment. Therefore, $EF_{\mathrm{emi}} = (EF_{\mathrm{emi},x} + EF_{\mathrm{emi},y})/2$, where $EF_{\mathrm{emi},x}$ and $EF_{\mathrm{emi},y}$ are the emission enhancement factors for the dipole moment perpendicular and parallel to the NW, respectively.

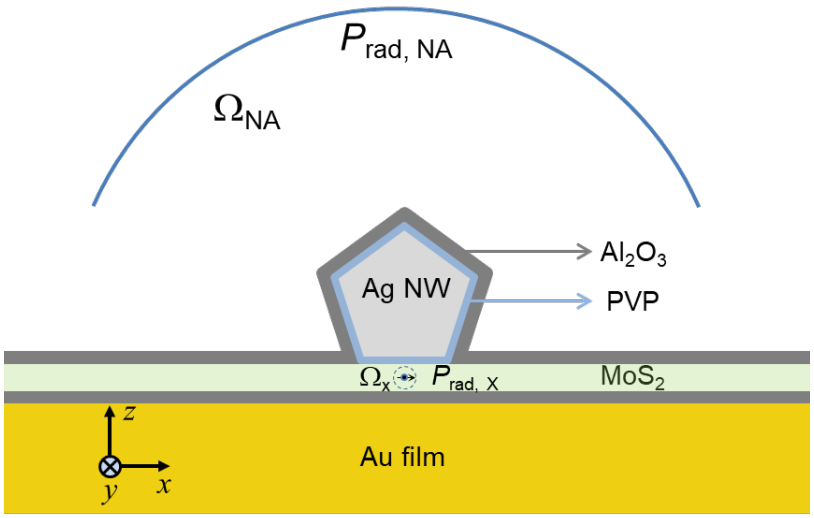

Fig. S9 Schematic diagram for simulating the emission. The surface Ω_X encloses an oscillating current source with the radiated power $P_{rad, X}$. The surface Ω_{NA} represents the far-field integration surface with a solid angle corresponding to the numerical aperture of the objective, and the power radiated over the surface Ω_{NA} is $P_{rad, NA}$. In the simulation of the emission enhancement, the imaginary part of the permittivity of the MoS_2 layer is removed.

The enhancement factor of the MoS_2-NWOM coupled system is evaluated by taking account of the contribution from each point underneath the NW. The points are spaced by 1.25 nm and distributed underneath one half of the NW because the enhancement factors are the same for the other half due to the symmetry of the MoS_2-NWOM coupled system. The excitation enhancement factor is

$$\overline{EF}_{exc} = \left(\int_0^{D/2} EF_{exc} dL \right) / (D/2), \tag{S5}$$

the emission enhancement factor is

$$\begin{aligned} \overline{EF}_{emi} &= \left(\int_0^{D/2} EF_{emi} dL \right) / (D/2) \\ &= \left(\int_0^{D/2} \frac{EF_{emi, x} + EF_{emi, y}}{2} dL \right) / (D/2), \\ &= \left(\overline{EF}_{emi, x} + \overline{EF}_{emi, y} \right) / 2 \end{aligned} \tag{S6}$$

and the PL enhancement factor is

$$\overline{EF}_{\mathrm{PL}} = \frac{\int_0^{D/2} |\mathbf{E}_x + \mathbf{E}_y|^2 \cdot QY \cdot \eta dL}{\int_0^{D/2} |\mathbf{E}_{x,\,\mathrm{film}} + \mathbf{E}_{y,\,\mathrm{film}}|^2 \cdot QY_{\mathrm{film}} \cdot \eta_{\mathrm{film}} dL}, \tag{S7}$$

where D is the diameter of the NW.

Fig. S10 shows the simulation results of the excitation enhancement factor as a function of NW diameter. For the laser light polarized perpendicular to the NW, the excitation enhancement factor is much larger than that for parallel polarization for both excitation wavelengths of 532 nm and 633 nm.

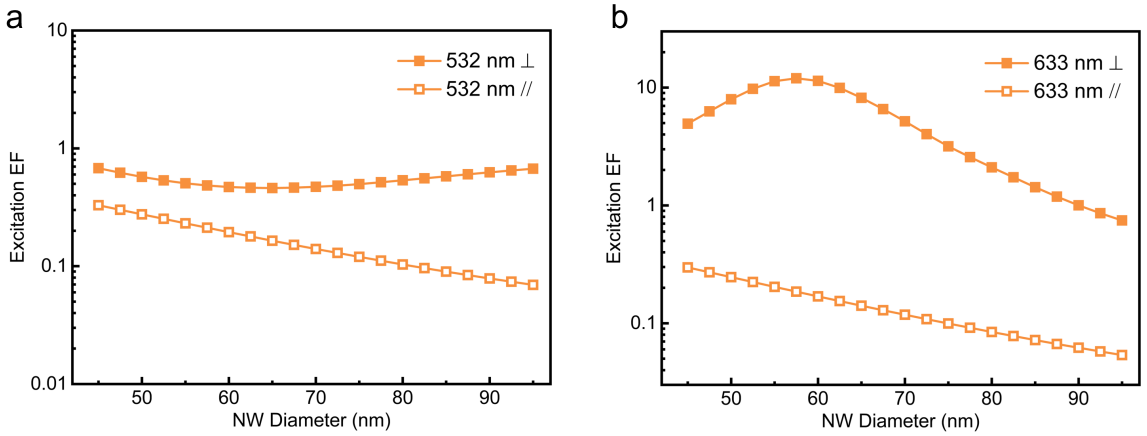

Fig. S10 Simulated results of excitation enhancement factor (EF) as a function of NW diameter for excitation wavelengths of 532 nm (a) and 633 nm (b). The excitation light is polarized perpendicular (solid squares) and parallel (hollow squares) to the NW.

Fig. S11 shows the simulation results of the emission enhancement factor for *x*- and *y*-orientated dipoles ($\overline{EF}_{\mathrm{emi},x}$ and $\overline{EF}_{\mathrm{emi},y}$) as a function of NW diameter. When the dipole moment is perpendicular to the NW, the emission is enhanced and the maximum enhancement is reached for the NW diameter of 70 nm. When the dipole moment is parallel to the NW, the emission is suppressed. Therefore, the emission enhancement factor of the coupled system is dominated by the *x*-oriented dipoles.

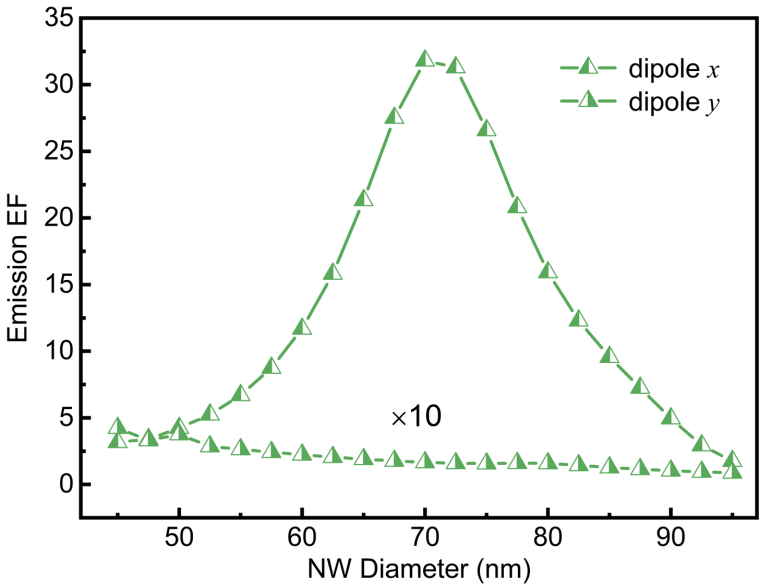

Fig. S11 Simulated results of $\overline{EF}_{\mathrm{emi},x}$ and $\overline{EF}_{\mathrm{emi},y}$ as a function of NW diameter. The values for *y*-oriented dipoles are magnified ten times.

In the calculation of the emission enhancement, the intrinsic quantum yield of monolayer MoS_2 QY_0 is set to be 0.01%.[9] Fig. S12 shows the emission enhancement factor for three different values of QY_0. As can be seen, the value of QY_0 doesn't have a large influence on the emission enhancement factor for the very low quantum yield considered here.

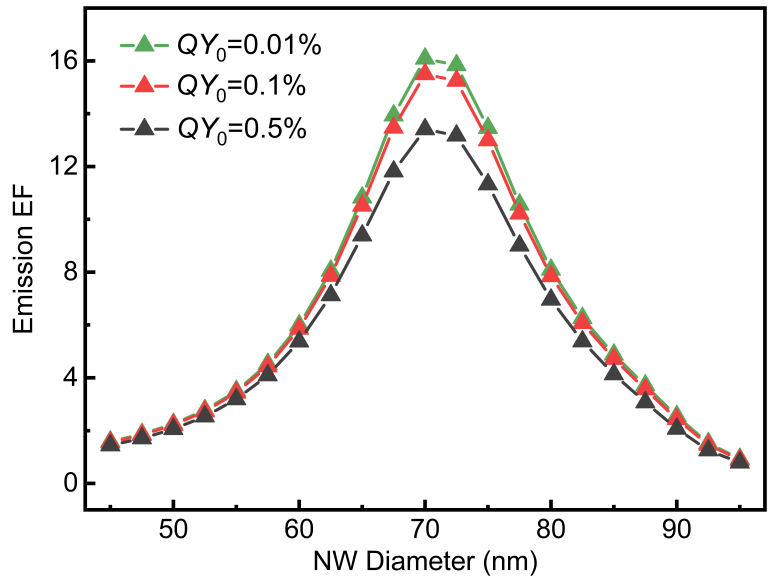

Fig. S12 Simulated results of $\overline{EF}_{\mathrm{emi}}$ as a function of NW diameter with different values of intrinsic quantum yield of monolayer MoS_2.

Fig. S13a and b show the PL enhancement factor for *x*- and *y*-oriented dipoles with the excitation light polarized perpendicular to the NW. These results indicate that the PL enhancement factor of the coupled system is dominated by the *x*-oriented dipoles. The PL enhancement factor for excitation of parallel polarization is much smaller than that for perpendicular polarization, as shown in Fig. S13c and d. The simulated results agree with the experimental results in Fig. S6a and b and Fig. S7b and c.

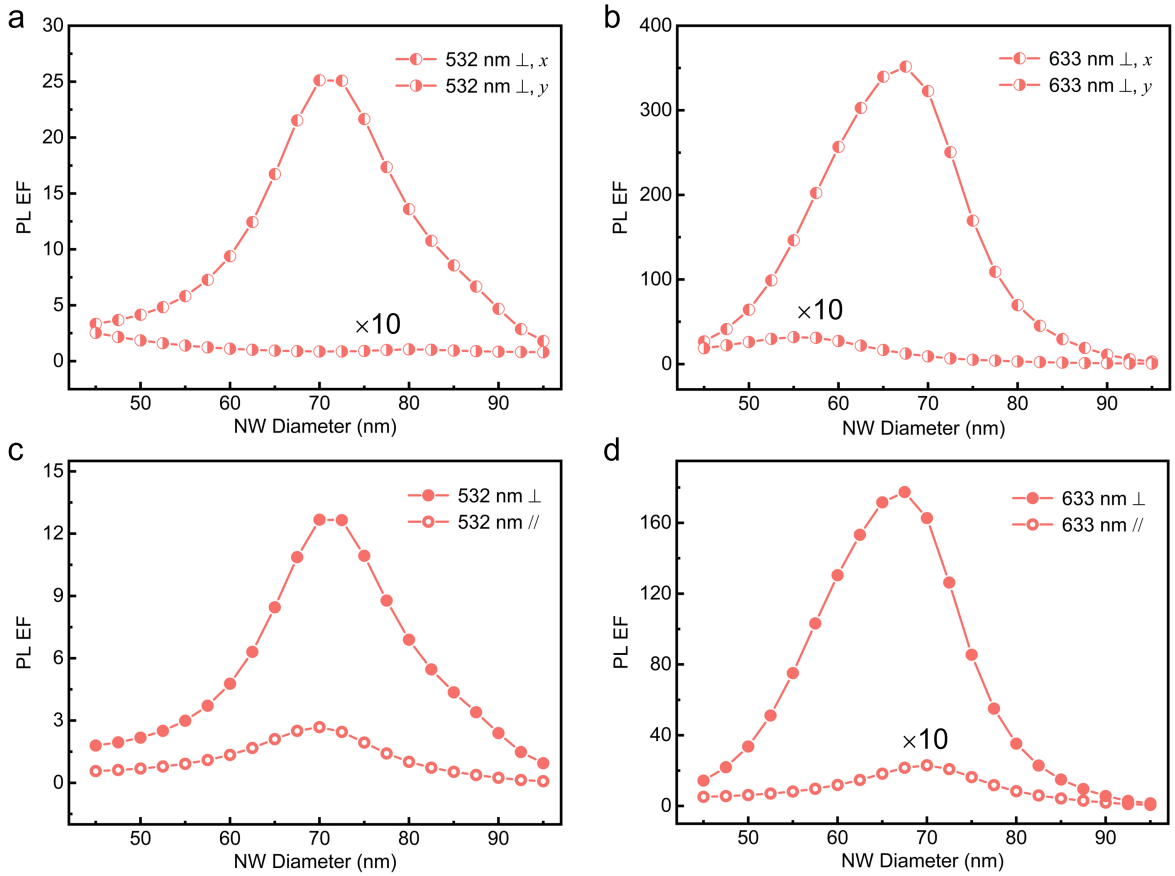

Fig. S13 (a and b) Simulated results of PL enhancement factor as a function of NW diameter for dipole moment perpendicular (*x*) and parallel (*y*) to the NW. The excitation light is polarized perpendicular to the NW. The values for *y*-oriented dipoles are magnified ten times. (c and d) Simulated results of PL enhancement factor as a function of NW diameter with the excitation light polarized perpendicular (solid dots) and parallel (hollow dots) to the NW. The values for parallel excitation in (d) are magnified ten times. The excitation wavelengths are 532 nm (a and c) and 633 nm (b and d).

The PL enhancement factor can be related with the excitation and emission enhancement

factors as follows:

$$\overline{EF}_{\mathrm{PL}} = \frac{\int_0^{D/2} |\mathbf{E}_x + \mathbf{E}_y|^2 \cdot QY \cdot \eta dL}{\int_0^{D/2} |\mathbf{E}_{x,\,\mathrm{film}} + \mathbf{E}_{y,\,\mathrm{film}}|^2 \cdot QY_{\mathrm{film}} \cdot \eta_{\mathrm{film}} dL} = f\,\overline{EF}_{\mathrm{exc}}\,\overline{EF}_{\mathrm{emi}}, \tag{S8}$$

where f is a factor which may depend on the excitation and emission wavelengths and the geometry of the MoS_2-NWOM coupled system. Since the emission enhancement factor $\overline{EF}_{\mathrm{emi}}$ is the same for excitation light of 532 nm and 633 nm, the excitation enhancement factor for 633 nm excitation can be written as

$$\overline{EF}_{\mathrm{exc},\,633} = g\,\overline{EF}_{\mathrm{PL},\,633} / \overline{EF}_{\mathrm{PL},\,532}, \tag{S9}$$

where $g = f_{532}\,\overline{EF}_{\mathrm{exc},\,532} / f_{633}$. As shown in Fig. S14, the value of g is close to 1. Therefore, equation (S9) can be approximated as

$$\overline{EF}_{\mathrm{exc},\,633} \approx \overline{EF}_{\mathrm{PL},\,633} / \overline{EF}_{\mathrm{PL},\,532}. \tag{S10}$$

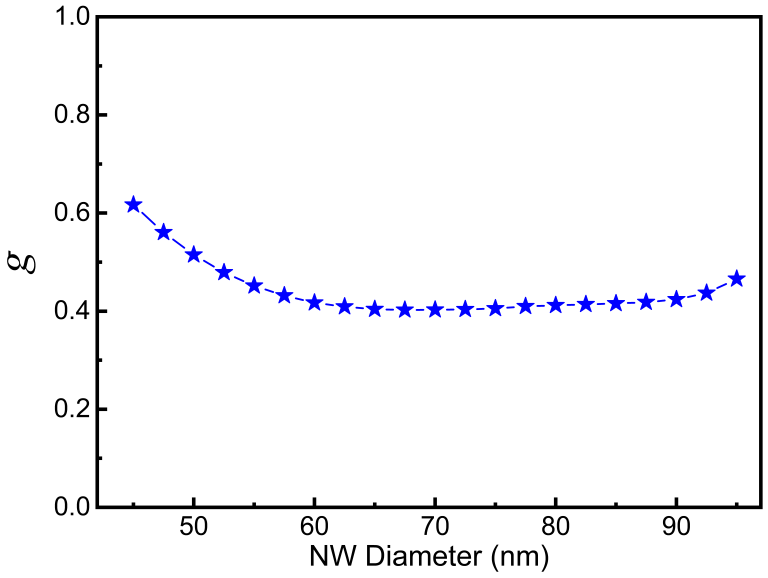

Fig. S14 Simulated results of g as a function of NW diameter.

To calculate the DOLP of the emission light, the components of the radiation polarized perpendicular or parallel to the NW are extracted. The emission intensity for different polarizations is proportional to $\frac{|\mathbf{E}_x + \mathbf{E}_y|^2 P_{\mathrm{rad,\,NA},j}}{P_{\mathrm{rad,\,X}} + P_{\mathrm{rad},\,0}(1-QY_0)/QY_0}$ for the dipole with x or y

orientation at each point, where j represents the emission polarization perpendicular (⊥) or parallel (//) to the NW. It is then position-averaged to mimic the emission intensity of the experimental system. Fig. S15a shows the calculated emission intensity for the dipoles with *x* or *y* orientation as a function of NW diameter. As can be seen, the intensity of the emission polarized perpendicular to the NW from the *x*-oriented dipoles dominates the PL intensity of the coupled system and shows similar dependence on the NW diameter as the PL enhancement factor (see Fig. S13d). Considering the emission from dipoles of both orientations, the intensity of the emission polarized perpendicular to the NW is more strongly dependent on the NW diameter compared with the intensity of the emission polarized parallel to the NW, as can be seen in Fig. S15b. The intensity ratio of the emission polarized perpendicular and parallel to the NW gets to the maximum when the NW diameter is about 67.5 nm (Fig. S15c), corresponding to the maximum DOLP.

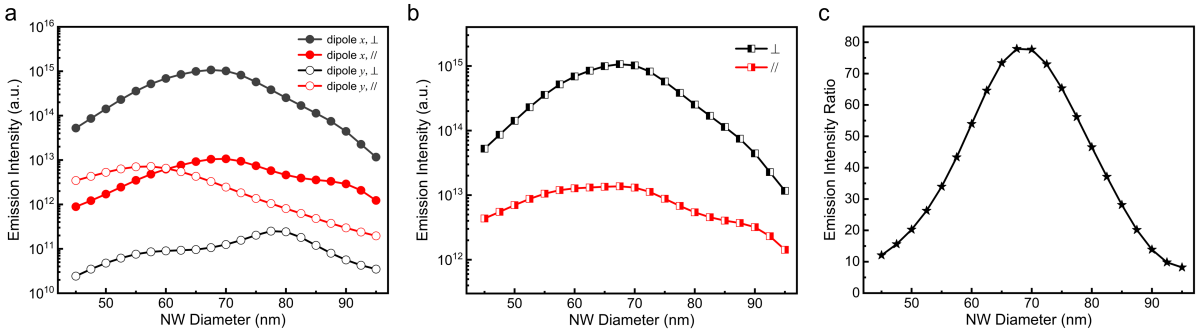

Fig. S15 (a) Simulated results of emission intensity for the polarization perpendicular (black) and parallel (red) to the NW as a function of NW diameter for dipole moment perpendicular (*x*, solid dots) and parallel (*y*, hollow dots) to the NW. (b) Simulated results of emission intensity for the polarization perpendicular (black half-filled squares) and parallel (red half-filled squares) to the NW from both *x*- and *y*-orientated dipoles as a function of NW diameter. (c) Intensity ratio of the emission polarized perpendicular and parallel to the NW. The excitation light is of 633 nm wavelength and polarized perpendicular to the NW.

References

1. W. Chen, P. Roelli, A. Ahmed, S. Verlekar, H. T. Hu, K. Banjac, M. Lingenfelder, T. J. Kippenberg, G. Tagliabue and C. Galland, *Nat. Commun.*, 2021, **12**, 2731.

2. Y. J. Niu, L. Gao, H. X. Xu and H. Wei, *Nanophotonics*, 2023, **12**, 735-742.
3. R. Boidin, T. Halenkovič, V. Nazabal, L. Beneš and P. Němec, *Ceram. Int.*, 2016, **42**, 1177-1182.
4. T. A. F. König, P. A. Ledin, J. Kerszulis, M. A. Mahmoud, M. A. El Sayed, J. R. Reynolds and V. V. Tsukruk, *ACS Nano*, 2014, **8**, 6182-6192.
5. P. B. Johnson and R. W. Christy, *Phys. Rev. B*, 1972, **6**, 4370-4379.
6. T. W. Lo, Q. Zhang, M. Qiu, X. Y. Guo, Y. J. Meng, Y. Zhu, J. J. Xiao, W. Jin, C. W. Leung and D. Y. Lei, *ACS Photonics*, 2019, **6**, 411-421.
7. W. Li, A. G. Birdwell, M. Amani, R. A. Burke, X. Ling, Y. H. Lee, X. L. Liang, L. M. Peng, C. A. Richter, J. Kong, D. J. Gundlach and N. V. Nguyen, *Phys. Rev. B*, 2014, **90**, 195434.
8. M. Pelton, *Nat. Photonics*, 2015, **9**, 427-435.
9. S. Roy, A. S. Sharbirin, Y. J. Lee, W. B. Kim, T. S. Kim, K. Cho, K. Kang, H. S. Jung and J. Kim, *Nanomaterials*, 2020, **10**, 1032.